

Electric polarization induced by phase separation in magnetically ordered and paramagnetic states of RMn_2O_5 ($R = \text{Gd}, \text{Bi}$)

B.Kh. Khannanov^{a,*}, V.A. Sanina^{a,**}, E.I. Golovenchits^a, M.P. Scheglov^a

^a*A.F. Ioffe Physical Technical Institute RAS, 26 Politekhnikeskaya, 194021, St. Petersburg, Russia*

Abstract

The electric polarization hysteresis loops and remanent polarization were revealed in multiferroics RMn_2O_5 with $R = \text{Gd}$ and Bi at wide temperature interval from 5 K up to 330 K. Until recently, the long-range ferroelectric order having an exchange-striction magnetic nature had been observed in RMn_2O_5 only at low temperatures ($T \leq T_C = 30 - 35$ K). We believe that the polarization we observed was caused by the frozen superparaelectric state which was formed by the restricted polar domains resulting from phase separation and charge carriers self-organization. At some sufficiently high temperatures $T \gg T_C$ the frozen superparaelectric state was destroyed, and the conventional superparaelectric state occurred. This happened when the potential barriers of the restricted polar domain reorientations become equal to the kinetic energy of the itinerant electrons (leakage). The hysteresis loops were measured by the so-called PUND method which allowed us to correctly subtract the contribution of conductivity from the measured polarization. The correlations between properties of the phase separation domains and polarization were revealed and studied. The high-temperature polarization also had a magnetic nature and was controlled by the magnetic field because the double exchange between pairs of Mn ions with different valences (Mn^{3+} and Mn^{4+}) in RMn_2O_5 was the basic interaction resulting in phase separation.

Keywords: multiferroic, polarization hysteresis loop, phase separation, charge carrier self-organization

PACS: 75.85.+t, 77.22.Ej, 77.80.Dj

1. Introduction

Manganites RMn_2O_5 (R are rare earth ions, Y and Bi) are typical representatives of multiferroics in which ferroelectric (with $T_C \approx 30 - 35$ K) and magnetic (with $T_N \approx 35 - 40$ K) orderings coexist [1–5]. It has been assumed until now that RMn_2O_5 has a centrosymmetric sp. gr. *Pbam* which forbids the existence of electric polarization. The ferroelectric ordering along the b axis at low temperatures is induced by charge and magnetic orders which break the central symmetry of the crystal due to the exchange-striction mechanism [6]. It has recently been shown [7] that the real RMn_2O_5 symmetry at room temperature is a noncentral symmetry which means that the electric polarization should exist at room

temperature. The authors could not give preference to one of two possible space groups: *P2* (allowing polarization along the c axis) and *Pm* (allowing polarization in the ab plane) on the basis of structural studies. By assuming from the physical considerations that the *homogeneous* electric polarization could exist at all temperatures only in one direction (i.e., along the b axis), they preferred the sp. gr. *Pm*. The authors [7] did not discuss the nature of this polarization. In [8] it was reported that the hysteresis loops of electric polarization and remanent polarization were detected in GdMn_2O_5 in a wide temperature range 5 – 330 K. We interpreted this polar state as a frozen superparaelectric state induced by *local polar domains* formed in the main crystal matrix due to phase separation and charge carriers self-organization. Theoretically, the frozen superparaelectric state was considered in the system of isolated ferroelectric nanoscale domains in a dielectric matrix [9].

This paper presents a comparative study of the electric polarization hysteresis loops which were revealed in

*Corresponding author

**Principal corresponding author

Email addresses: boris.khannanov@gmail.com

(B.Kh. Khannanov), sanina@mail.ioffe.ru (V.A. Sanina), e.golovenchits@mail.ioffe.ru (E.I. Golovenchits), m.scheglov@mail.ioffe.ru (M.P. Scheglov)

two crystals of the RMn_2O_5 family with $R = \text{Gd}$ and Bi in temperature interval from 5 K up to 330 K. There are significant structural distortions in BiMn_2O_5 caused by Bi ions due to the presence of alone pairs of $6s^2$ electrons [10]. The Bi^{3+} ions are nonmagnetic ones but they strongly distort the lattice, while strongly magnetic Gd^{3+} ions with the ground state ($^8S_{7/2}$) interact weakly with the lattice. Of particular interest is the correlation between the properties of phase separation domains and electrical polarizations in these two model crystals. Magnetization, electric polarization, permittivity, and conductivity studies and also features of high-resolution X-ray diffraction scattering of RMn_2O_5 ($R = \text{Gd}, \text{Bi}$) are reported.

A characteristic feature of RMn_2O_5 is the presence of equal amounts of manganese ions with different valences Mn^{3+} (containing $3t_{2g}$, $1e_g$ electrons in the $3d$ shell) and Mn^{4+} (with $3t_{2g}$, $0e_g$ electrons), which provides conditions for charge ordering. The Mn^{4+} ions have an octahedral oxygen environment and are arranged in the layers with $z = 0.25c$ and $(1 - z) = 0.75c$. The Mn^{3+} ions have a local non-central surrounding in the form of a pentagonal pyramid and are arranged in the layers with $z = 0.5c$. The R^{3+} ions have the environment similar to that of the Mn^{3+} ions and are arranged in the layers $z = 0$ [11]. Charge ordering in RMn_2O_5 and the e_g electron transfer between Mn^{3+} - Mn^{4+} ion pairs (double exchange [12, 13]) are key factors responsible for polar electric states of these multiferroics at all temperatures. The low-temperature ferroelectric ordering in RMn_2O_5 is caused by charge ordering of alternating Mn^{3+} - Mn^{4+} ion pairs with antiferromagnetically and ferromagnetically oriented spins along the b axis. Different values of indirect exchange between the antiferromagnetic Mn^{3+} - Mn^{4+} ion pairs and considerably stronger double exchange between the ferromagnetic pairs of these ions lead to the exchange striction that breaks the centrosymmetry of the lattice, thus giving rise to the ferroelectric polarization along the b axis at $T \leq T_C$ [6, 11].

The double exchange between Mn^{3+} - Mn^{4+} ions induces phase separation in RMn_2O_5 which is similar to phase separation in LnAMnO_3 ($A = \text{Sr}, \text{Ba}, \text{Ca}$) manganites containing Mn^{3+} and Mn^{4+} ions as well. Phase separation exists at all temperatures and makes the formation of local conductive domains containing Mn^{3+} - Mn^{4+} ion pairs with ferromagnetically oriented spins energetically favorable. The phase separation domains are located in a dielectric antiferromagnetic (paramagnetic) matrix of the original crystal. The size and geometry of the local phase separation domains are determined by a dynamic balance of interactions which

leads to the attraction of charge carriers (double exchange, the Jahn-Teller effect) and Coulomb repulsion [13, 14]. The effect of phase separation domains on the RMn_2O_5 properties was studied from 5 K up to the temperatures above room temperature. At $T < T_C$ the phase separation domains manifested themselves as 1D superlattices with alternating ferromagnetic layers containing different numbers of charge carriers. It was supposed that these superlattices were multiferroic domain walls (with their own polarizations) located between ferroelectric domains of the basic crystal matrix. A set of ferromagnetic resonances from individual superlattice layers was detected for a number of multiferroics RMn_2O_5 ($R = \text{Eu}, \text{Gd}, \text{Er}, \text{Tb}, \text{Bi}$) [15–17]. In the paramagnetic and paraelectric temperature range, up to temperatures above room temperature, the polar nature of local phase separation domains was found to be responsible for dielectric properties and the features of the high-resolution X-ray diffraction spectra of RMn_2O_5 ($R = \text{Eu}$ and Gd) single crystals [18–20]. The 2D superstructures of alternating layers of the initial RMn_2O_5 crystals and phase separation domains were revealed at sufficiently high temperatures. Most distinctly these superstructures (perpendicular to the c axis) manifested themselves in the X-ray studies of EuMn_2O_5 and $\text{Eu}_{0.8}\text{Ce}_{0.2}\text{Mn}_2\text{O}_5$ at room temperature. The superstructure layer thicknesses were 900 Å and 700 Å, respectively [18, 19].

2. Experimental

Single crystals of RMn_2O_5 were grown by the spontaneous crystallization technique described in [21, 22]. The as-grown single crystals were in the form of 2 – 3 mm thick plates with areas of 3 – 5 mm². To measure the polarization, capacitors with a thickness of 0.3 – 0.6 mm and area of 3 – 4 mm² were used. The electric polarization was measured by two methods, i.e., the thermo-stimulated pyrocurrent method and the so-called positive-up negative-down (PUND) method of hysteresis loops measuring [23–25]. In the first case the polarization was measured by a Keithly 6514 electrometer and the measurements were produced during sample heating with a constant temperature variation rate after the preliminary sample cooling in a polarizing electric field which was switched off at the lowest temperature. In the second case we employed the version of the PUND method presented in [25] which was adapted to our measurements (see Fig. 1 in [8]). If the sample had a relatively high conductivity (which is important for RMn_2O_5 containing restricted polar phase separation domains with local conductivities), the shape

of the polarization – electric field (P-E) hysteresis loop was distorted and did not give correct information on the intrinsic polarization P. In the PUND method only the hysteresis of P can be extracted by applying a series of voltage pulses to the sample. During successive positive P1-P2 and negative N1-N2 pulses, independent curves (P1-P2 and N1-N2) of effective polarization P changes are registered. The PUND method is based on the difference between polarization and conductivity responses to variations in the field E. The time intervals between P1-P2 and N1-N2 pulses should be chosen such that the intrinsic polarization P is still unrelaxed, while the conductivity relaxation is complete. In the conventional volume ferroelectrics with the domain structure those time intervals may be up to seconds. In our case the intrinsic P response was determined by the restricted polar phase separation domains which rather rapidly restored after the field E was switched off. The reason for this will be discussed below. As a result,

tion contribution) and the conductivity responses to the P2 and N2 pulses were closed and reversible (see Fig. 1 in [8]). This could be achieved if the time intervals between the P1-P2 and N1-N2 pulses did not exceed 0.8 ms. The P1 and N1 curves characterized the total polarization and conductivity contributions. To obtain the actual P-E loop, we subtracted the P2 and N2 curves from the P1-N1 curves. The durations of pulses in the P1-P2 and N1-N2 series were 2 ms and 4.5 ms, the intervals between the pulse series were 4 ms and 9 ms for GdMn_2O_5 and BiMn_2O_5 , respectively. The permittivity and conductivity were measured by a Good Will LCR-819 impedance meter in the frequency range 0.5 – 50 kHz at 5 – 350 K. Magnetic properties were investigated by PPMS (Quantum Design). The intensity distributions of Bragg reflections were studied with a high-sensitivity 3-crystal X-ray diffractometer.

3. Experimental results and analysis

3.1. Magnetic properties and low-temperature ferroelectric state

Complicated magnetic structures with wave vector $q = (1/2 + \delta x, 0, 1/4 + \delta z)$ and a number of low-temperature magnetic phase transitions at $T \leq T_N$ at which incommensuration parameters δx and δz change in a step-like fashion are typically observed in RMn_2O_5 with different R ions [11]. As temperature decreases, an incommensurate magnetic phase is appeared near T_N . At a lower temperature this phase is transformed into a commensurate structure. As temperature further decreases, one more transition into the incommensurate phase is possible. Ferroelectric ordering in RMn_2O_5 is typically occurs in the intermediate commensurate phase.

Magnetic structures of GdMn_2O_5 and BiMn_2O_5 differ from those commonly observed in RMn_2O_5 . In GdMn_2O_5 , a commensurate collinear antiferromagnetic structure with wave vector $q = (1/2, 0, 0)$ occurs in the temperature range 0 – 30 K [26]. At these temperatures there is a ferroelectric ordering with $T_C \approx 30$ K. In the temperature range $35 \text{ K} \geq T > 30$ K there is an incommensurate phase. In BiMn_2O_5 the commensurate noncollinear antiferromagnetic structure with $q = (1/2, 0, 1.2)$ is observed at $T \leq T_N \approx 40$ K [11, 27]. Fig. 1 shows temperature dependence of magnetization in magnetic field $H = 5$ kOe along different axes of the GdMn_2O_5 (Fig. 1a) and BiMn_2O_5 (Fig. 1b) crystals studied. It can be seen that the magnetic moment in GdMn_2O_5 is much higher due to the contribution of Gd^{3+} ions with the $S = 7/2$ spin which have their own

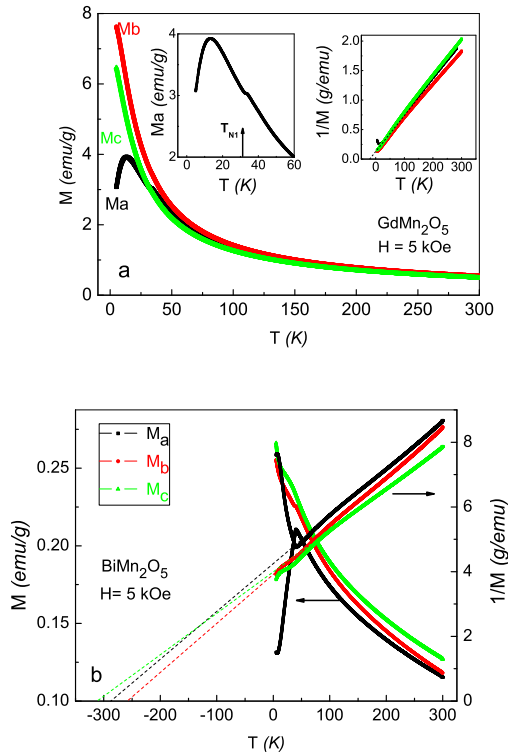


Figure 1: Temperature dependences of magnetization along all crystal axes for GdMn_2O_5 (a) and BiMn_2O_5 (b).

the time intervals between the P1-P2 and N1-N2 pulses were chosen so that the responses to the P1 and N1 pulses were irreversible (due to the intrinsic polariza-

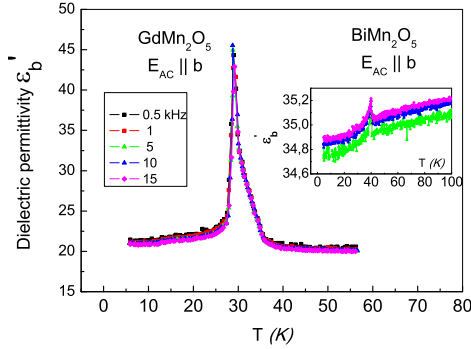


Figure 2: Dispersion-free anomalies of real permittivity ϵ' along the b axis at $T \approx T_C$ for GdMn_2O_5 and BiMn_2O_5 (in the inset).

ordering at $T \approx 13$ K. On the background of magnetization of Gd ions, the antiferromagnetism of manganese ions along the a axis (with $T_N = 35$ K) manifests itself only slightly (see the left inset in Fig. 1a). The right inset in Fig. 1a shows that the Curie-Weiss temperature for GdMn_2O_5 nearly coincides with T_N . This means that there is a distinct phase transition near T_N in GdMn_2O_5 (the magnetic state is not frustrated). A quite different magnetic state is observed in BiMn_2O_5 (Fig. 1b). The antiferromagnetism along the c axis manifests itself only slightly, while it is pronounced along the a axis. Unlike in GdMn_2O_5 , but similar to RMn_2O_5 with other R ions, the Curie-Weiss temperature exceeds $T_N = 40$ K in 6-7 times. This means that the magnetic state in BiMn_2O_5 is highly frustrated, and spin correlations in local domains are observed at $T \gg T_N$. Specific magnetic and structural properties of BiMn_2O_5 in the RMn_2O_5 family are caused by the presence of electron lone pairs in Bi^{3+} ions.

High-resolution neutron powder diffraction studies [27] show that BiMn_2O_5 is characterized at room temperature by the orthorhombic sp. gr. $Pbam$, similar to other RMn_2O_5 . However, Mn^{4+} -O6 octahedra, Mn^{3+} -O5 pyramids, and Bi^{3+} -O units are more deformed as compared with those in other RMn_2O_5 . As a result, the Mn-O distances and magnetic exchange bonds differ as well.

As will be shown below, differences in magnetic and structural states of GdMn_2O_5 and BiMn_2O_5 lead to different electric polarizations at all temperatures. Let us consider at first the low-temperature polar states. Fig. 2 shows dispersion-free anomalies of real permittivity ϵ' along the b axis which are characteristic of the low-temperature ferroelectric phase transition. As one can see, the value of ϵ' at the maximum in the

vicinity of T_C in GdMn_2O_5 considerably exceeds the maximum in BiMn_2O_5 . Fig. 3 shows electric polarizations along the b axis (P_b) in GdMn_2O_5 (Fig. 3a) and BiMn_2O_5 (Fig. 3b). The polarizations are measured by the pyrocurrent method on the assumption that $P_b = 0$ at $T \geq T_C$. The maximum polarization P_b (in our case $P_b \approx 0.26 \mu\text{C}/\text{cm}^2$) for the RMn_2O_5 family is observed in GdMn_2O_5 [26]. In BiMn_2O_5 , polarization P_b is an order of magnitude lower and is closer to the values typically observed in other RMn_2O_5 [5]. Note that a fully

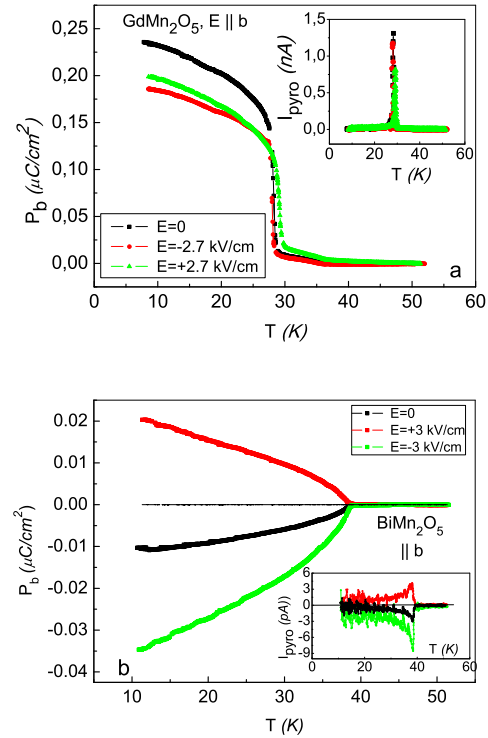


Figure 3: Temperature dependences of polarizations P_b and pyrocurrents along the b axis at $E = 0$ and $E \neq 0$ for GdMn_2O_5 (a) and BiMn_2O_5 (b).

polarized state is often observed in structurally perfect (according to X-ray diffraction) RMn_2O_5 single crystals with different R ions in the absence of an applied external electric field E [28]. This indicates that this fully polarized P_b polarization is formed in the internal field. We suppose that this is a staggered-like field caused by charge ordering of Mn^{3+} - Mn^{4+} ion pairs along the b axis, and the polarization has an exchange-striction nature. This situation is observed for both crystals we studied. In GdMn_2O_5 (Fig. 3a), the maximum polarization is detected in $E = 0$. A uniform external field $\pm E \parallel b$ which is much weaker than the internal

staggered-like field, only slightly reduces polarization P_b and cannot reverse its orientation (Fig. 3a). The application of a strong field $E \parallel b$ (comparable to the internal field) enhances the transfer of e_g valence electrons between the Mn^{3+} - Mn^{4+} ion pairs along the b axis, which leads to the electric breakdown of the crystal. Therefore, measurements of the polarization hysteresis loops P_b (which are the response to an applied external field E) is not effective when the striction contribution to the GdMn_2O_5 polarization at $T < T_C$ is measured. In BiMn_2O_5 (which are also structurally perfect single crystals), Bi ions distort the uniformity of the internal staggered-like field, thus reducing its value and, hence, the exchange-striction polarization P_b . In this case application of field $\pm E \parallel b$ changes the internal field to a greater extent and can even reverse the BiMn_2O_5 polarization (see Fig. 3b). As can be seen, the application of E in the same direction in which the polarization was observed at $E = 0$ enhances the polarization by the value close to that detected in E of the opposite orientation (Fig. 3b). There is good reason to believe that the internal exchange-striction polarization is the polarization observed at $E = 0$. There are two additional contributions to the polarization of BiMn_2O_5 in the case of application of field $E \parallel b$. There is the contribution originating from a weak change in the internal staggered-like-field and that due to the response of phase separation domains to the applied field E . Note that the polarization measured by the pyrocurrent method includes the contribution of conductivities of phase separation domains.

3.2. Polarization hysteresis loops for GdMn_2O_5 and BiMn_2O_5

As noted above, it was shown in [8] that electric polarization hysteresis loops in GdMn_2O_5 were observed in a wide temperature interval (from the lowest up to room temperature). We put forward the hypothesis that this polarization was due to the frozen superparaelectric state of restricted polar phase separation domains formed in the initial crystal matrix. Phase separation must exist in RMn_2O_5 with any R ions at all temperatures, but the phase separation domain states depend on the R ion type and temperature. Thus, two electric polarizations having different natures (the long-range ferroelectric order with polarization P_b caused by exchange striction and the polarization due to polar phase separation domains) must coexist in RMn_2O_5 along the b axis at $T \leq T_C$. The previous subsection was concerned with the polarizations P_b at $T \leq T_C$ measured by the pyrocurrent method at $E = 0$ in GdMn_2O_5 (Fig.3a) and

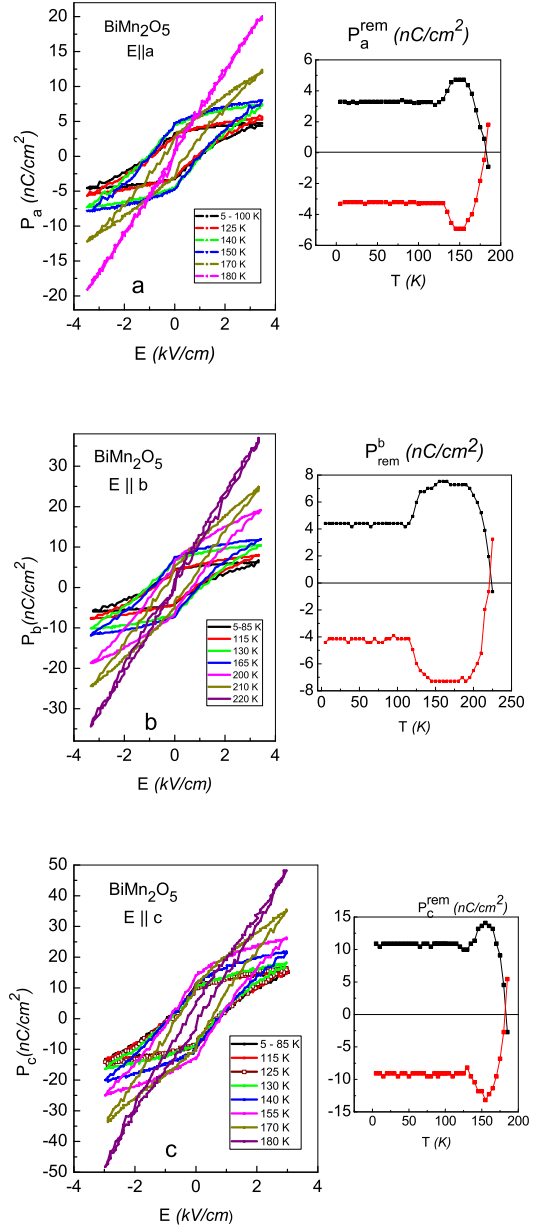


Figure 4: Polarization hysteresis loops for BiMn_2O_5 (left panels) at different temperatures at $E \parallel a$ (a), $E \parallel b$ (b), and $E \parallel c$ (c). Temperature dependences of remanent polarization are shown in right panels.

BiMn_2O_5 (Fig. 3b). This polarization gave no contribution to the hysteresis loops which were responses to the applied field E . On the contrary, the polarization caused by phase separation domains could be determined only by measuring the hysteresis loops by the PUND method that excluded the contribution of conductivity. By using

these two methods, we could separate the contributions of the polarizations considered above at low temperatures.

Let us consider in more detail the hysteresis loops for BiMn_2O_5 in a wide temperature interval and compare them with the loops for GdMn_2O_5 . Fig. 4 shows the P-E hysteresis loops of BiMn_2O_5 in E oriented along the a , b , and c axes (left panels in Figs. 4a, 4b, and 4c, respectively). The right panels in these figures demonstrate temperature dependences of the remanent polarization (P^{rem}). Figs. 5a, 5b, and 5c present the P-E hysteresis loops and P^{rem} for GdMn_2O_5 . As one can see, the hysteresis loops are observed for both crystals along all three axes from 5 K up to some temperatures T^* which depend on the axis direction. The maximum P^{rem} polarizations are observed along the c axis from 5 K up to $T^* \approx 180$ K in BiMn_2O_5 and up to $T^* \approx 325$ K for GdMn_2O_5 . The minimum P^{rem} along the b axis which exists up to $T^* \approx 100$ K is observed for GdMn_2O_5 , while a twice higher P^{rem} along the b axis for BiMn_2O_5 manifests itself up to $T^* \approx 220$ K. The P^{rem} along the a axis are observed for GdMn_2O_5 and BiMn_2O_5 up to $T^* \approx 295$ K and $T^* \approx 180$ K, respectively. Thus, P^{rem} and hysteresis loops for BiMn_2O_5 and GdMn_2O_5 which demonstrate a strong anisotropy are revealed in the paramagnetic phase. It is important to note that the polarizations of both crystals occurred along all crystal axes and disappeared at different temperatures along these axes. This fact means that the polarizations measured in the hysteresis loops were not caused by the ferroelectric phase transition in the homogeneous ferroelectric crystal states. As noted above, we assumed that these polarizations were induced by the restricted polar phase separation domains. It turned out that these polarizations were significantly lower than the exchange-striction ferroelectric low-temperature polarization along the b axis at $T \leq T_C$.

The remanent polarization P^{rem} along the b axis (Fig. 5b) in GdMn_2O_5 is two orders of magnitude lower than the exchange-striction contribution of the basic crystal matrix polarization P_b at $T < 30$ K measured by the pyrocurrent method in the same sample at $E = 0$ (Fig. 3a). The contribution of P_b into the hysteresis loops manifests itself only in the form of maxima on the background of P_b^{rem} near T_C when the internal staggered-like-field which gives rise to polarization P_b begins to decrease and disappears and the P_b fluctuations increase (see Fig. 5b). There is no exchange-striction polarization of the main matrix in the direction of the a and c axes at $T \leq T_C$, and therefore contributions to the hysteresis loops come only from phase separation domains at all temperatures. The fact that

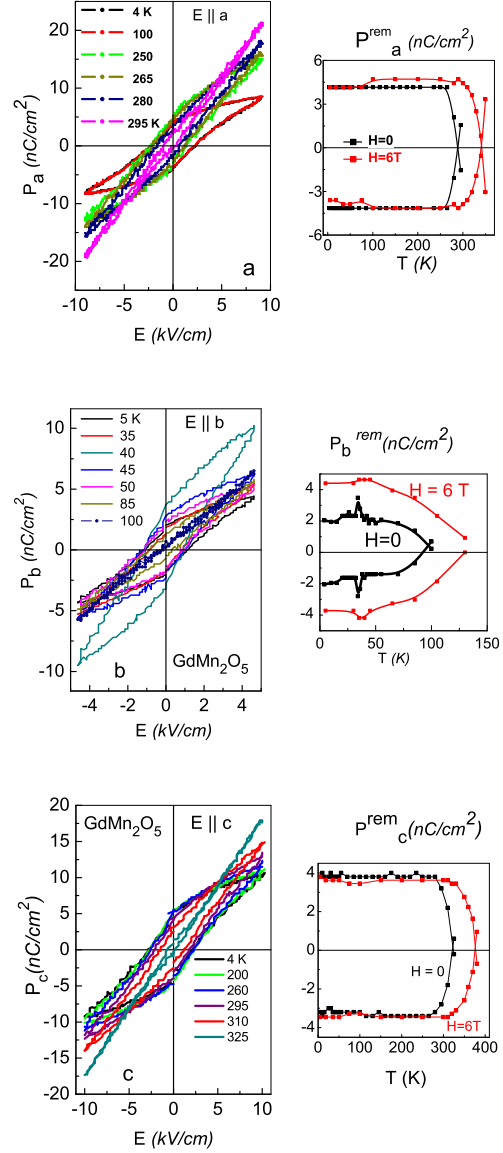


Figure 5: Polarization hysteresis loops for GdMn_2O_5 (left panels) at different temperatures at $E \parallel a$ (a), $E \parallel b$ (b), and $E \parallel c$ (c). Temperature dependences of remanent polarization are shown in right panels.

P^{rem} is independent of temperature along all axes of GdMn_2O_5 in a wide temperature range (for the b axis this relates to the background value minus the maxima near T_C) indicates that the contribution into the polarization from phase separation domains in GdMn_2O_5 is anisotropic but temperature-independent. At T^* the remanent polarizations rather abruptly disappear along different crystal axes. Of interest is the fact that, unlike in GdMn_2O_5 , the P^{rem} values along all axes of the

BiMn_2O_5 crystal abruptly increase in the vicinity of $T \approx 125$ K and then rapidly reduce to zero near the T^* . Such P^{rem} jumps near 125 K indicate that phase separation domain states in BiMn_2O_5 should change in a step-like fashion near this temperature. The absence of such jumps in GdMn_2O_5 shows that most probably these jumps in BiMn_2O_5 result from structural lattice distortions caused by the Bi ions.

The effect of the longitudinal magnetic field H on the hysteresis loops was also studied. As one can see from the right panels in Fig. 5, the field $H = 6$ T increases in GdMn_2O_5 both the remanent polarization and temperature T^* along the b axis and only T^* along the a and c axes.

Characteristic activation barriers E_A must exist at the interfaces between phase separation domains and the main matrix of the crystal. Information on E_A along different crystal axes can be obtained from frequency-temperature dependences of real permittivity ϵ' and conductivity σ . Fig. 6 shows the $\epsilon'(T)$ and $\sigma(T)$ dependences for BiMn_2O_5 at different frequencies along the a axis (Fig. 6a), b axis (Fig. 6b), and c axis (Fig. 6c). It is evident that the values of ϵ' and σ along all axes of the crystal are nearly independent of temperature at $T \leq 125$ K. Near $T \approx 125$ K a frequency-dependent step-like ϵ' increase to some constant level (most pronounced along the a and b axes) begins. As temperature further grows, ϵ' starts to increase sharply again. The frequency-dependent growth of σ also begins near 125 K, and two the different temperature intervals of σ increase are observed as well. Note that the temperature independence of ϵ' and σ at $T \leq 125$ K and similar steps in the $\epsilon'(T)$ and $\sigma(T)$ dependences near 125 K correlate with the temperature dependences of P^{rem} in BiMn_2O_5 along different crystal axes (see Fig. 4). Indeed, near $T \approx 125$ K P^{rem} increases in a step-like fashion along all axes of the crystal. The temperatures at which the second high-temperature growth in ϵ' and σ start are close to T^* for different crystal axes. The temperatures of ϵ' jumps at different frequencies at $T^* > T > 125$ K are well described by the Arrhenius law, which allows one to estimate characteristic activation barriers E_A at the phase separation domain boundaries in BiMn_2O_5 . These values are close to 0.3 eV along different crystal axes (see Fig. 6).

Let us turn to a more detailed examination of the conductivity of the crystals. We deal with the real conductivity $\sigma_1 = \omega \epsilon'' \epsilon_0$ [29] which is calculated from dielectric losses ϵ'' (ω is the angular frequency, ϵ_0 is the permittivity ϵ' at $\omega = 0$). This conductivity depends on both the frequency and temperature. The low-frequency conductivities are dispersion-free (per-

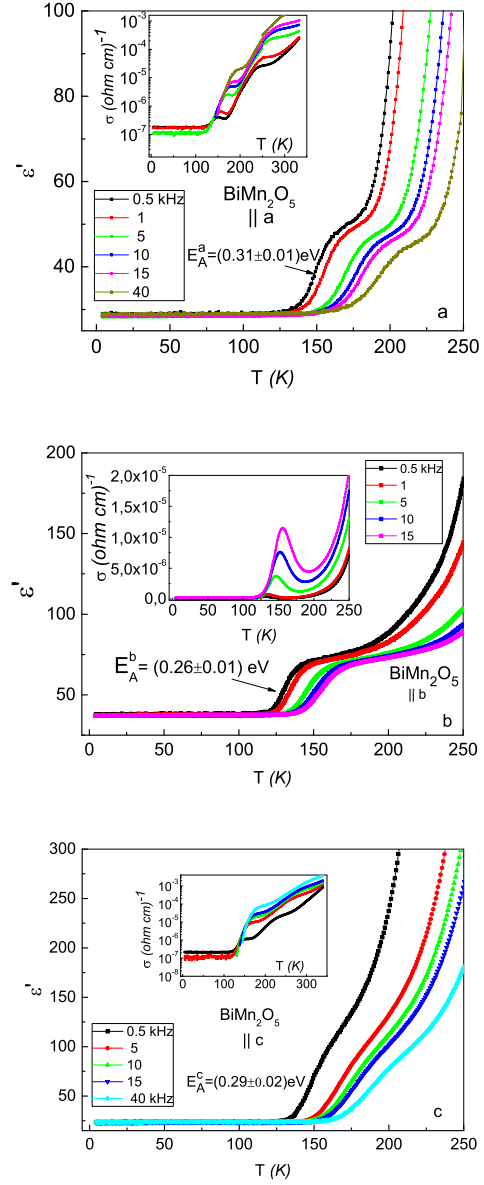


Figure 6: Temperature dependences of the real permittivity ϵ' and conductivity σ (in insets) at different frequencies for BiMn_2O_5 along the a axis (a), b axis (b), and c axis (c).

colation conductivity σ_{dc}). The conductivity σ_{ac} has a frequency dispersion: the higher the frequency, the higher the conductivity. The frequency dispersion of this type is typical of local conductivity (i.e., dielectric losses) in restricted domains [29]. In our case, we attributed this local conductivity to phase separation domains. The percolation conductivity (leakage) is attributable to the initial crystal matrix. The relative

local conductivity $\sigma_{loc} = (\sigma_{ac} - \sigma_{dc})/\sigma_{dc}$ characterizes the ratio between the phase separation domain local conductivity and matrix leakage. Fig. 7 shows σ_{loc} for BiMn_2O_5 along the a , b , and c axes (Figs. 7a, 7b, and 7c, respectively). Along the b axis only one, most intense, maximum in σ_{loc} in the temperature interval 125 – 220 K is observed. Below 100 K σ_{loc} also exists, but at $T > 100$ K it is transformed into leakage, and near 125 K it again becomes a local conductivity (see the inset in Fig. 7b). The activation barrier calculated from the shifts of the local conductivity maxima at $T > 125$ K (Fig. 7b) exceeds E_A^b derived from the ε' jumps only slightly (Figs. 6b and 7b). At $T < 100$ K the conductivities along the a and c axes were low and could not be measured correctly by our device. There are two σ_{loc} maxima along these axes at $T > 125$ K, the first is in the same temperature interval 125 – 220 K as along the b axis; the second is in the temperature region 225 – 350 K. The presence of two maxima split in temperature along the a and c axes in BiMn_2O_5 means that the leakage sharply increases in the temperature interval between the maxima. Such behaviors of σ_{loc} along the a and c axes correlate with the temperature behaviors of ε' along these axes (Fig. 4). However, the activation barriers calculated from the shifts of the first maxima of σ_{loc} are almost twice as high as the barriers derived from the ε' jumps (compare Fig. 6 and Fig. 7). The inset in Fig. 8 shows temperature dependences of conductivities of GdMn_2O_5 along the b and c axes at different frequencies. The conductivity along the a axis is close to that along the c axis. Of interest is the fact that the frequency-dependent conductivity jumps along the a and c axes in GdMn_2O_5 also emerge near 125 K, like in BiMn_2O_5 . The activation barrier E_A in GdMn_2O_5 calculated from the conductivity jumps is 0.2 eV. Fig. 8 shows the temperature intervals in GdMn_2O_5 in which σ_{loc} of the phase separation domains exceeds considerably the matrix leakage. Conductivity σ_{loc} along the b axis manifests itself up to $T \approx 125$ K. At $T > 125$ K there is only the leakage which grows with temperature. At $T \approx 125$ K σ_{loc} along the a and c axes rises abruptly and exists up to room temperature without a noticeable change. The hysteresis loops and P^{rem} along all axes in both crystals are screened by leakage rather sharply at the temperatures T^* at which the leakage and local conductivities become comparable. This means that the T^* values correspond to the temperatures at which the potential barriers of the restricted polar domain reorientations become equal to the kinetic energy of the itinerant electrons (leakage).

Differences between polar properties of phase separation domains in GdMn_2O_5 and BiMn_2O_5 are observed

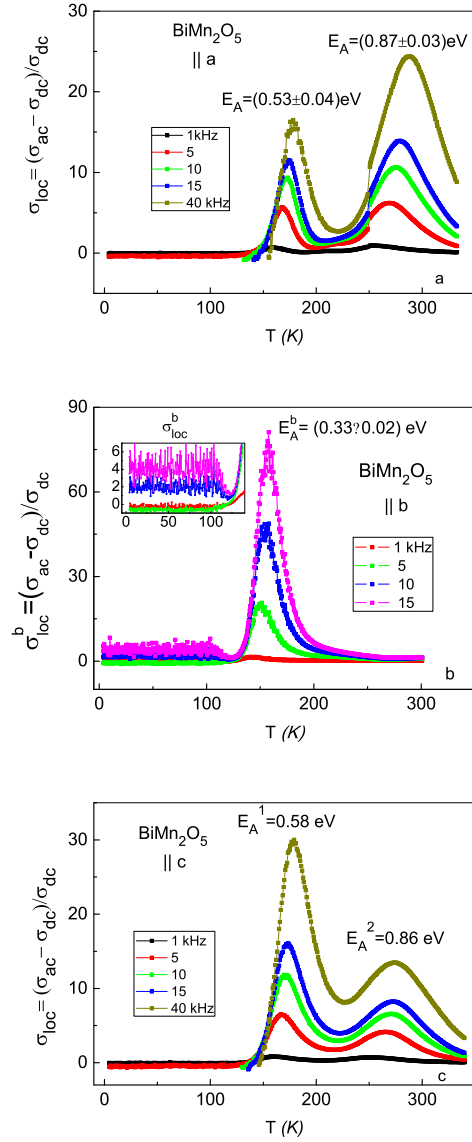


Figure 7: Temperature dependences of σ_{loc} at different frequencies for BiMn_2O_5 along the a axis (a), b axis (b), and c axis (c). Inset shows the same dependences along the b axis at $T < 125$ K at a larger scale.

along all axes of the crystals at $T > 125$ K. At $T < 125$ K the ground states of phase separation domains are similar for both crystals, which means that these states are formed inside the Mn subsystems under the barriers of any origin. Near 125 K the leakage and local conductivities along the b axes become comparable in both crystals. The itinerant electrons which appear along the b axes at $T > 125$ K are localized anew in deeper potential wells thus passing into σ_{loc} of the phase separation

domains. In GdMn_2O_5 these σ_{loc} exceed leakage up to T^* equal to 295 K and 325 K along the a and c axes, respectively (see Fig. 5). In BiMn_2O_5 σ_{loc} of phase separation domains emerges at $T > 125$ K along all crystal axes, including the b axis, due to the effect of Bi ions. The localization of itinerant electrons in potential wells leads to deepening of these wells and increases the activation barriers of phase separation domains. These E_A barriers can be calculated from the shifts of the temperature maxima of σ_{loc} at different frequencies. Indeed, these barriers in BiMn_2O_5 turned out to be twice as high as E_A calculated from the ε' jumps. The latter barriers correspond to the condition when the kinetic energy of the itinerant electrons emerging along the b axis becomes comparable to E_A calculated from the ε' jumps. The values of T^* in BiMn_2O_5 along different axes correlate with the temperatures at which the conductivity at the lowest frequency (leakage) begins to increase sharply in the first σ_{loc} maxima (compare Fig. 4 and Fig 7). Note that near $T_C \approx 30$ K dispersion-free

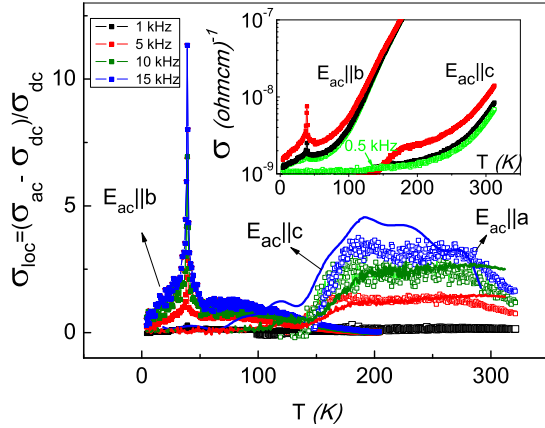


Figure 8: Temperature dependences of σ_{loc} for GdMn_2O_5 along all axes (the a axis — unfilled symbols, the b axis — filled symbols, the c axis — lines) for different frequencies. The inset shows temperature dependences of conductivity along the b and c axes for different frequencies.

anomalies typical of the ferroelectric phase transition manifest themselves in GdMn_2O_5 on the background of σ_{loc} and σ_{ac} along the b axis (see Fig. 8). This is due to the fact that a maximum in ε'' should be observed near T_C , while in BiMn_2O_5 a low polarization P_b does not manifest itself on the background of σ_{loc} (Fig. 7b).

Both the intrinsic polarization and σ_{loc} of restricted polar phase separation domains give contributions into the P1 and N1 curves in measurements of hysteresis loops for GdMn_2O_5 and BiMn_2O_5 at $T < T^*$ by the PUND method, while σ_{loc} contributes significantly to the P2 and N2 curves in the same temperature interval.

At these temperatures P^{rem} emerges in these crystals. Near T^* at which P^{rem} tends to zero, the polarization and local conductivity contributions to the P1-P2 and N1-N2 curves start to decrease simultaneously. At the temperatures at which $P^{rem} = 0$, these contributions are transformed into linear dependences on E . At $T > T^*$ the loop restores as an inverted loop, and the leakage contribution begins to dominate in it.

3.3. X-ray high-sensitivity diffraction study

The experimental evidence of the existence of restricted polar phase separation domains of GdMn_2O_5 and BiMn_2O_5 was obtained in the X-ray high-sensitivity diffraction study carried out at room temperature (see Figs. 9a and 9b, respectively). The angular intensity distributions of (004) , (060) and $(600)_{CuK\alpha 1}$ Bragg reflections were detected in the 3-crystal regime with the $\theta/2\theta$ scan. As a monochromator and an analyzer, germanium crystals in the (004) reflection were used, which allowed conditions of nearly dispersion-free high-resolution ($\sim 2''$) survey geometry to be realized. Fig. 9a shows a single diffraction maximum of (060) and two diffraction maxima of the (004) Bragg reflections recorded from different planes of a single crystal of GdMn_2O_5 . These planes are perpendicular to the b and c axes, respectively. The (004) Bragg reflection positions are characterized by slightly different interplanar spacings d ($\Delta d \approx 0.0015$ Å). These (004) reflections, which have comparable intensities and half-widths ($\sim 20''$) clearly point to the coexistence of two phases with slightly differing c lattice parameters which differ in the third decimal place. The Bragg peak along the b axis with a similar half-width is not split, i.e., it is identical to these two phases. The positions of all Bragg peaks nearly coincide with those for GdMn_2O_5 with the generally accepted $Pbam$ symmetry. This means that two phases we detected are high-quality GdMn_2O_5 single crystal phases with similar large correlation lengths R_c . The phase with a higher intensity of the (004) Bragg peak can be attributed to the original matrix. The phase with a lower intensity of such a peak can be attributed to the phase separation domains. A similar picture of the angular intensity distributions of the (004) , (060) and $(600)_{CuK\alpha 1}$ Bragg reflections is also observed for BiMn_2O_5 , but splitting into two peaks for the reflexes along all axes of the crystal is detected (Fig. 9b). It is natural to attribute this to lattice distortions caused by Bi ions along all crystal axes. Note that the structural quality of both crystals is similar.

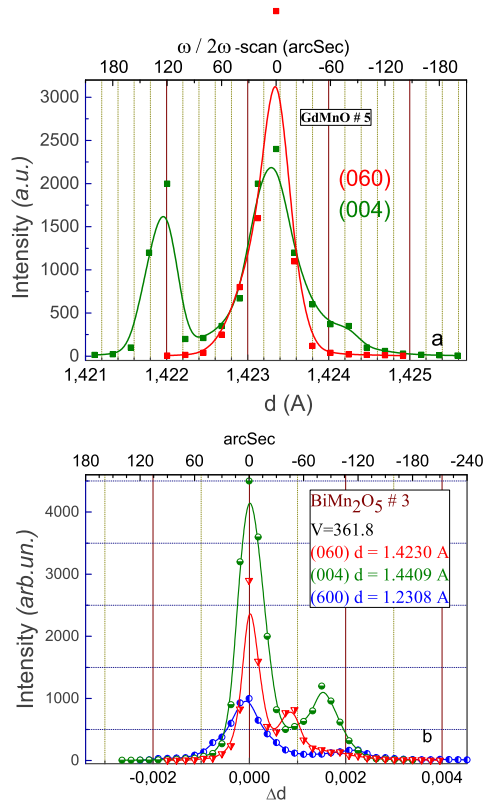


Figure 9: Angular intensity distributions of (600) , (060) , and $(004)_{CuK\alpha1}$ Bragg reflections as functions of interplanar distances (d Å) in $GdMn_2O_5$ (a) and $BiMn_2O_5$ (b). Parameters of $GdMn_2O_5$ lattice are $a = 7,3568 \pm 0.0002$ Å; $b = 8,5398 \pm 0.0002$ Å; $c = 5,6920 \pm 0.0002$ Å.

3.4. Discussion

Let us discuss the shape and structure of phase separation domains in $GdMn_2O_5$ and $BiMn_2O_5$. As noted above, the phase separation domains in the form of 1D superlattices were observed below the temperatures of magnetic and ferroelectric orderings in a number of RMn_2O_5 with various R ions, including $R = Gd$ and Bi [15–17]. A set of ferromagnetic resonances was detected from individual layers of superlattices. The intensity of these resonances sharply decreased when $T \approx 30 - 40$ K was approached. Since the phase separation domains should exist at all temperatures, this fact means that the structure of the phase separation domains must change at $T > 40$ K. We manage to study the temperature evolution of ferromagnetic resonances of layered superlattices at $T > 40$ K only in $Eu_{0.8}Ce_{0.2}Mn_2O_5$, in which the phase separation domains were similar to those in $EuMn_2O_5$, but their concentration was much high [18, 19]. In temperature interval $100 K > T > 40$ K only one ferromagnetic res-

onance signal was observed in $Eu_{0.8}Ce_{0.2}Mn_2O_5$. This resonance corresponded to the low-temperature superlattice layer having the maximal barrier and conductivity [16]. Near 100 K an intensity of this resonance became indistinguishable due to growth of conductivity. At room temperature the structure of phase separation domains was installed in $Eu_{0.8}Ce_{0.2}Mn_2O_5$ in X-ray diffraction study [18]. The two (004) well defined Bragg peaks were accompanied by the characteristic oscillation peaks independent on the interplanar spacings d , which pointed to existence of the layered superstructure in this crystal. As shown in [18], the layered superstructure consisting of the alternating original crystal $EuMn_2O_5$ layers and conductive layers of phase separation emerged in $Eu_{0.8}Ce_{0.2}Mn_2O_5$ at all temperatures above 40 K. No similar oscillation peaks on the background of the Bragg reflexes were observed in X-ray studies of $GdMn_2O_5$ and $BiMn_2O_5$ at room temperature (Fig. 9), i.e., there were no layered superstructures in these crystals. Most likely the phase separation domains in $GdMn_2O_5$ and $BiMn_2O_5$ had the shape of nanoscale droplets at $T > 40$ K. The possibility of different geometries of the phase separation domains in Coulomb-frustrated systems, including manganites and high-temperature superconductors, was shown theoretically in [30–32]. The properties of the phase separation domains in the form of nanoscale droplets for manganites were discussed in [13, 14].

Now consider in more detail what are polar phase separation domains. There is a probability that e_g electrons of some Mn^{3+} ions tunnel to Mn^{4+} ions in the original RMn_2O_5 matrix. These valence electrons and recharged $Mn^{3+}-Mn^{4+}$ ion pairs are accumulated in the restricted phase separation domains inside the original matrix because phase separation is energetically favorable [13, 14]. Since Mn^{3+} ions appear in the Mn^{4+} ion positions (i.e., in the octahedral oxygen surrounding), they become Jahn-Teller ions and give rise to local deformations of these octahedra. In turn, Mn^{4+} ions appear in the Mn^{3+} ion positions (in noncentrosymmetrical pentagonal pyramids) and local distortions arise near these ions as well. As a result, structural distortions caused by both these factors occur inside restricted phase separation domains. We believe that phase separation domains are noncentrosymmetric, and their sizes are large enough to give rise to ferroelectric single-domain states inside them.

The restricted polar phase separation domain states existing in $GdMn_2O_5$ and $BiMn_2O_5$ original matrices are analogs of the superparaelectric state formed by an ensemble of spherical ferroelectric nanoparticles in a dielectric matrix theoretically studied in [9]. It was

shown in [9] that at low temperatures a homogeneous polarization could exist in these particles (in our case restricted polar phase separation domains) if their sizes R were less than the correlation radius R_c but larger than the critical radius R_{cr} of the size-driven ferroelectric-paraelectric phase transition. Under these conditions all dipole moments inside particles are aligned due to correlation effects. Surface screening of depolarization fields makes single-domain states energetically favorable. If $R < R_{cr}$, separate paraelectric dipoles are uncorrelated and represent local polar defects which can only increase the width of the Bragg peak original matrix. The fact that the well-defined Bragg reflections related to the restricted polar phase separation domains are observed in our study together with similar Bragg peaks of the original matrix indicates that the conditions for the ferroelectric single-domain states of phase separation regions given in [9] are fulfilled. It was also found in [9] that a frozen superparaelectric phase could emerge for an ensemble of ferroelectric nanoparticles in a dielectric matrix. In this phase remanent polarization and hysteresis loop arose at the temperatures lower than the freezing temperature T_f . T_f was defined from the condition that the potential barriers of nanoparticle polarization reorientation became equal to the thermal activation energy $\sim k_B T$. At $T > T_f$ the conventional superparaelectric state occurred for which there are no hysteresis loops and remanent polarization. It was also accepted in [9] that the temperature of thermal destruction of intrinsic nanoparticle ferroelectricity was $T_{cr} \gg T_f$. So, the temperature behavior of the GdMn_2O_5 and BiMn_2O_5 polarization is also analogous to that of the frozen superparaelectric state discussed in [9]. T^* considered above can be regarded as T_f . As noted above, the T^* values correspond to the temperatures at which the potential barriers of the restricted polar domain reorientations become equal to the kinetic energy of the itinerant electrons (leakage). The restricted phase separation domains still exist at $T > T^*$ due to energetic favorability of the phase separation caused by strong interactions. But the frozen superparaelectric state turns into the conventional superparaelectric one near T^* .

Since $P - E$ hysteresis loops are measured under the field E applied along different axes, electric polarizations inside phase separation domains are induced along these axes. Indeed, the application of field E along any crystal axis initiates a drift of valence e_g electrons localized inside phase separation domains in this direction. These electrons recharge Mn^{3+} and Mn^{4+} ions inside the phase separation domains. As a result, the spatial distribution of the Mn^{3+} and Mn^{4+} ions and structural

distortions inside phase separation domains are bound to change, thereby giving rise to the polarization along the E direction. Thus, the actual symmetry of RMn_2O_5 at room temperature can be established only in polarization measurements in $E = 0$. We believe that the additional structural reflexes typical of the noncentral monoclinic structure reported in [7] can be related to the frozen superparaelectric state arising in RMn_2O_5 at $T \leq T^*$. Note that in the cases when temperatures T^* are sufficiently high, the correlations between the phase separation domains can occur in the entire crystal volume. This situation was observed earlier in $\text{Eu}_{0.8}\text{Ce}_{0.2}\text{Mn}_2\text{O}_5$ at room temperature [18].

As noted above, phase separation and charge carrier self-organization give rise to a dynamic equilibrium of the phase separation domain states with a balance between attraction (double exchange, Jahn-Teller effect) and Coulomb repulsion of charge carriers [13, 14, 18]. The formation of the phase separation domains due to a balance between strong interactions leads to specific features in RMn_2O_5 properties. First, polar phase separation domains are bound to emerge up to high temperatures, thus giving rise to high-temperature polarization. Second, changes in polar phase separation domains under varying E rapidly relax to the dynamic equilibrium states after E is switched off. These features manifested themselves in our experiments and necessitated the use of the PUND method for measuring the polarization hysteresis loops which were discussed above.

The application of magnetic field H increases the barriers at the phase separation domain boundaries due to the double exchange growth, thus increasing the T^* temperatures in GdMn_2O_5 (see the right panels in Fig. 5). The field H oriented along the b axis in GdMn_2O_5 also enhances the polarization induced by the restricted polar domains due to the increasing probability of charge transfer between $\text{Mn}^{3+} - \text{Mn}^{4+}$ ion pairs with the greatest distance between them (see the caption to Fig. 9a). It was found that application of magnetic field $H = 6$ T to BiMn_2O_5 had a much weaker effect on phase separation domain properties and polarization than in GdMn_2O_5 because of strong structural distortions of the crystal field by Bi ions.

4. Conclusion

Thus, remanent polarizations and hysteresis loops originating from the frozen superparaelectric state of similar ferroelectric restricted polar phase separation domains arranged inside the initial matrix of RMn_2O_5 ($R = \text{Gd}$ and Bi) have been revealed in wide temperature intervals from 5 K up to T^* depending on the crys-

tal axis. The restricted polar phase separation domains emerge due to phase separation and charge carrier self-organization. At $T \approx T^*$ the potential barriers of the restricted polar domain reorientations become equal to the kinetic energy of the itinerant electrons (leakage). In GdMn_2O_5 , the polarization of this type emerges along the c axis up to $T^* \approx 325$ K. In BiMn_2O_5 , the maximum temperature $T^* \approx 220$ K is observed along the b axis. At $T \geq T^*$ the frozen superparaelectric state turns into the conventional superparaelectric one. The polarizations observed can be attributed to the magnetically induced polarizations since the magnetic double exchange between Mn^{3+} - Mn^{4+} ion pairs is the key interaction giving rise to the phase separation domain formation. The effect of magnetic field on these polarizations in GdMn_2O_5 demonstrates that the magnetoelectric coupling exists in the paramagnetic phase as well. Application of electric field E modifies the structure and shape of the phase separation domains, giving rise to the polarization along the E direction. Additional structural reflexes typical of the noncentral monoclinic structure reported in [7] can be related to the frozen superparaelectric state arising in RMn_2O_5 at $T \leq T^*$. In the cases when temperatures T^* are sufficiently high, the correlations between the phase separation domains can emerge in the entire crystal volume thus giving rise the noncentrosymmetry of the whole crystals.

5. Acknowledgments

The work was supported by the Government of Russian Federation (project N0.14.B25.31.0025).

References

- [1] T. Kimura, T. Goto, H. Shintani, K. Ishizaka, and Y. Tokura, Magnetic control of ferroelectric polarization, *Nature* (London) 426 (2003) 55-58 doi: 10.1038/nature02018.
- [2] N. Hur, S. Park, P.A. Sharma, J.S. Ahn, S. Guba, and S-W. Cheong, Electric polarization reversal and memory in a multiferroic material induced by magnetic fields, *Nature* (London) 429 (2004) 392-395. doi: 10.1038/nature02572.
- [3] H. Katsura, N. Nagaosa and A.V. Balatsky, Spin current and magnetoelectric effect in noncollinear magnets, *Phys. Rev. Lett.* 95 (2005) 057205. DOI: <http://dx.doi.org/10.1103/PhysRevLett.95.057205>
- [4] M. Mostovoy, Ferroelectricity in spiral magnets, *Phys. Rev. Lett.* 96 (2006) 067601 DOI: 10.1103/PhysRevLett.96.067601.
- [5] Y. Noda, H. Kimura, M. Fukunaga, S. Kobayashi, I. Kagomiya, and K. Kohn, Magnetic and ferroelectric properties of RMn_2O_5 , *J. Phys.: Condens. Matter* 20 (2008) 434206. DOI: <http://dx.doi.org/10.1088/0953-8984/20/43/434206>.
- [6] J. van den Brink and D.I. Khomskii, Multiferroicity due to charge ordering, *J. Phys.: Cond. Matter* 20 (2008) 434217. DOI: <http://dx.doi.org/10.1088/0953-8984/20/43/434217>.
- [7] V. Baledent, S. Chattopadhyay, P. Fertey, M.B. Lepetit, M. Greenblatt, B. Wanklyn, F.O. Saouma, J.I. Jang, and P. Foury-Leykian, Evidence for room temperature electric polarization in RMn_2O_5 , *Phys. Rev. Lett.* 114 (2015) 117601. DOI: <http://dx.doi.org/10.1103/PhysRevLett.114.117601>.
- [8] B.Kh. Khannanov, V.A. Sanina, E.I. Golovenchits, M.P. Scheglov, Room-temperature electric polarization induced by phase separation in multiferroic GdMn_2O_5 , *JETPLett* 103 (2016) 248-253. DOI: 10.1134/S002136401604007x.
- [9] M.D. Glinchuk, E.A. Eliseev, and A.N. Morozovska, Superparaelectric phase in the ensemble of non-interacting ferroelectric nanoparticles, *Phys. Rev. B.* 78 (2008) 134107. DOI: <http://dx.doi.org/10.1103/PhysRevB.78.134107>.
- [10] N.A. Hill, Why are there so few magnetic ferroelectrics?, *J. Phys. Chem. B* 104 (2000) 6694-6709. DOI: 10.1021/p000114x.
- [11] P.G. Radaelli and L.C. Chapon, A neutron diffraction study of RMn_2O_5 multiferroics, *J. Phys.: Condens. Matter* 20 (2008) 434213. DOI: <http://dx.doi.org/10.1088/0953-8984/20/43/434213>.
- [12] P.G. de Gennes, Effects of double exchange in magnetic crystals, *Phys. Rev.* 118 (1960) 141-153. DOI: <http://dx.doi.org/10.1103/PhysRev.118.141>.
- [13] L.P. Gor'kov, Lattice and magnetic effects in doped manganites, *Phys.-Usp.* 41 (1998) 589-594. DOI: 10.1070/PU1998v041n06ABEH000409.
- [14] M.Yu. Kagan and K.I. Kugel, Inhomogeneous charge distribution and phase separation in manganites, *Phys.-Usp.* 44 (2001) 553-570. DOI: 10.1070/PU2001v044n06ABEH000917.
- [15] E.I. Golovenchits, V.A. Sanina, V.G. Zaleskii, Spin-wave resonances in $\text{Eu}_{0.8}\text{Ce}_{0.2}\text{Mn}_2\text{O}_5$ and EuMn_2O_5 , *JETPLett.* 95 (2012) 386-390. DOI: 10.1134/S002136012070053.
- [16] V.A. Sanina, E.I. Golovenchits, V.G. Zaleskii, Spin-wave excitations in superlattices self-assembled in multiferroic single crystals, *J. Phys.: Cond. Matter* 24 (2012) 346002. DOI: <http://dx.doi.org/10.1088/0953-8984/24/34/346002>.
- [17] B.Kh. Khannanov, V.A. Sanina, E.I. Golovenchits, Giant polarization and magnetic dynamics in GdMn_2O_5 , *J. Phys. Conf. Ser.* 572 (2014) 012046. DOI: <http://dx.doi.org/10.1088/1742-6596/572/1/012046>.
- [18] V.A. Sanina, E.I. Golovenchits, V.G. Zaleskii, S.G. Lushnikov, M.P. Scheglov, S.N. Gvasaliya, A. Savinov, R.S. Katiyar, H. Kawaji, and T. Atake, Phase separation and charge carrier self-organization in semiconductor-multiferroic $\text{Eu}_{0.8}\text{Ce}_{0.2}\text{Mn}_2\text{O}_5$, *Phys. Rev. B* 80 (2009) 224401. DOI: 10.1103/PhysRevB.80.224401.
- [19] V.A. Sanina, E.I. Golovenchits, V.G. Zaleskii, and M.P. Scheglov, Magnetic properties of multiferroics-semiconductors $\text{Eu}_{0.8}\text{Ce}_{0.2}\text{Mn}_2\text{O}_5$, *J. Phys.: Cond. Matter* 23 (2011) 456003. DOI: <http://dx.doi.org/10.1088/0953-8984/23/45/456003>.
- [20] V.A. Sanina, E.I. Golovenchits, B.Kh. Khannanov, M.P. Scheglov, V.G. Zaleskii, Temperature evolution of the polar states in GdMn_2O_5 and $\text{Gd}_{0.8}\text{Ce}_{0.2}\text{Mn}_2\text{O}_5$, *JETPLett.*, 100 (2014) 407-412. DOI: 10.1134/S002136401418009x.
- [21] V.A. Sanina, L.M. Sapozhnikova, E.I. Golovenchits, and N.V. Morozov, Series of phase transitions in EuMn_2O_5 , *Sov. Phys. Solid State* 30 (1988) 1736-1742.
- [22] E.I. Golovenchits, N.V. Morozov, V.A. Sanina, and L.M. Sapozhnikova, Correlation of magnetic and dielectric properties of EuMn_2O_5 single crystals, *Sov. Phys. Solid State* 34 (1992) 56-59.
- [23] J.F. Scott, L. Kammerdiner, L.M. Parris, S. Traynor, V. Ottenbacher, A. Shawabkeh, and W.F. Oliver, Switching kinetics of lead zirconate titanate submicron thin-film memories, *J.Appl.Phys* 64 (1988) 787-792. DOI: <http://doi.org/10.1063/1.341925>.

- [24] M. Fukunaga and Y. Noda, New technique for measuring ferroelectric and antiferroelectric hysteresis loops, *J. Phys. Soc. J.* 77 (2008) 0647068 . DOI: <http://dx.doi.org/10.1143/JPSJ.77.064706>.
- [25] S.M. Feng, Y.S. Chai, J.L. Zhu, N. Manivannan, Y.S. Oh, L.J. Wang, Y.S. Yang, C.Q. Jin, and Kee Hoon Kim, Determination of the intrinsic ferroelectric polarization in orthorhombic HoMnO_3 , *New J. Phys.* 12 (2010) 073006. DOI: <http://iopscience.iop.org/1367-2630/12/7/073006>.
- [26] N. Lee, C. Vecchini, Y.J. Choi, L.C. Chapon, A. Bombardi, P.G. Radaelli, and S.W. Cheong, Giant tunability of ferroelectric polarization in GdMn_2O_5 , *Phys. Rev. Lett.* 110 (2013) 137203. DOI: 10.1103/PhysRevLett.110.137203.
- [27] A. Munoz, J.A. Alonso, M.T. Cosais, M.J. Martinez-Lope, J.L. Martinez, M.T. Fernandez-Diaz, Magnetic structure and properties of BiMn_2O_5 oxide: A neutron diffraction study, *Phys. Rev. B* 65 (2002) 144423. DOI: <http://dx.doi.org/10.1103/PhysRevB.65.144423>.
- [28] M. Fukunaga and Y. Noda, Measurement of complicated temperature-dependent polarization of multiferroics RMn_2O_5 , *J. Phys. Conf. Ser.* 320 (2011) 012090. DOI: <http://iopscience.iop.org/1742-6596/320/1/012090>.
- [29] A.R. Long, Frequency-dependent loss in amorphous semiconductors, *Adv. Phys.* 31 (1982) 587-637. DOI: 10.1080/0018738200101418.
- [30] C. Ortix, J. Lorenzana, and C. Di Castro, Coulomb-frustrated phase separation in systems with short-range negative compressibility, *Phys. Rev. Lett.* 100 (2008) 246402. DOI: <http://dx.doi.org/10.1103/PhysRevLett.100.246402>.
- [31] C. Ortix, J. Lorenzana, and C. Di Castro, Coarse grained models in Coulomb frustrated phase separation, *J. Phys.: Cond. Matter* 20 (2008) 434229. DOI: <http://dx.doi.org/10.1088/0953-8984/20/43/434229>.
- [32] K.I. Kugel, A.L. Rakhmanov, A.O. Sboychakov, F.V. Kusmartsev, Nicola Poccia, and Antonio Bianconi, A two-band model for the phase separation induced by the chemical mismatch pressure in different cuprate superconductors, *Semicond. Sci. Technol.* 22 (2009) 014007. DOI: <http://dx.doi.org/10.1088/0953-2048/22/1/014007>.